Geophysical Research Letters®

Key Points:
- Immediate foreshocks are observed for 527 Ridgecrest earthquakes
- Characteristics of their P waves do not scale with the eventual earthquake magnitudes
- These Ridgecrest earthquakes may have initiated as a rate-dependent cascading process

Correspondence to:
H. Meng,
h2meng@ucsd.edu

Immediate Foreshocks Indicating Cascading Rupture Developments for 527 M 0.9 to 5.4 Ridgecrest Earthquakes

Haoran Meng[1] and **Wenyuan Fan[1]**

[1]Scripps Institution of Oceanography, UC San Diego, La Jolla, CA, USA

Abstract Understanding earthquake foreshocks is essential for deciphering earthquake rupture physics and can aid seismic hazard mitigation. With regional dense seismic arrays, we identify immediate foreshocks of 527 $0.9 \leq M \leq 5.4$ events of the 2019 Ridgecrest earthquake sequence, including 48 earthquakes with series of immediate foreshocks. These immediate foreshocks are adjacent to the mainshocks occurring within 100 s of the mainshocks, and their P waves share high resemblances with the mainshock P waves. However, attributes of the immediate-foreshock P waves, including the amplitudes and preceding times, do not clearly scale with the mainshock magnitudes. Our observations suggest that earthquake rupture may initiate in a universal fashion but evolves stochastically. This indicates that earthquake rupture development is likely controlled by fine-scale fault heterogeneities in the Ridgecrest fault system, and the final magnitude is the only difference between small and large earthquakes.

Plain Language Summary Understanding earthquake foreshocks have both scientific and societal implications regarding earthquake physics and seismic hazards. Using dense arrays in the Ridgecrest region, we find immediate foreshocks of 527 earthquakes that occurred within a month of the 2019 M_w 7.1 Ridgecrest earthquake. These immediate foreshocks are adjacent to their mainshocks and likely near-instantaneously trigger the following slip within 100 s. Attributes of the P waves of these immediate foreshocks do not seem to correlate with the mainshock magnitudes. Our observations suggest that earthquakes may initiate via similar means and it remains challenging to use such foreshocks to predict the mainshock magnitudes.

1. Introduction

Identifying and observing geophysical signals of slip events preceding earthquakes have been of paramount importance because of their direct linkage with earthquake nucleation and rupture processes (e.g., Bouchon et al., 2013; Kanamori & Cipar, 1974; Liu et al., 2020; Ohnaka, 1992). Understanding such signals will offer insight into earthquake physics, but more importantly, knowledge of the signals can help hazard forecasting and mitigation (Mclaskey & Yamashita, 2017; Pritchard et al., 2020). The quest for short-term earthquake prediction has been paved with failed attempts, yet remains controversial (Dascher-Cousineau et al., 2020; Gulia & Wiemer, 2019; Kanamori, 2003; Sykes et al., 1999). This is because the observed preceding signals are often reported after the earthquakes and the examinations are not systematic, leaving the physical relations between these slip events and the mainshocks elusive. In practice, these signals are often difficult to identify without prior knowledge (Kanamori, 2003; Sykes et al., 1999). However, anomalous earthquake swarms and aseismic slips preceding the 2011 Tohoku-Oki and 2014 Iquique earthquakes show promising apparent precursors that can be observed to draw connections to the final megathrust ruptures (Kato et al., 2012; Ruiz et al., 2014). Yet, the consistency of such precursory signals is unclear, which hampers their practical implementations for operational warning purposes (Mignan, 2012, 2014).

Earthquake foreshocks are one type of possible precursors and their spatiotemporal correlation with the mainshocks suggests that they may help to describe the earthquake rupture preparation process (Kato et al., 2012; Moutote et al., 2021; Ruiz et al., 2014; Trugman & Ross, 2019). However, the general prevalence of foreshocks is less clear and the physical origin of the foreshocks is not well-understood (Abercrombie & Mori, 1996; Ellsworth & Bulut, 2018; Moutote et al., 2020; Seif et al., 2019; Shearer & Lin, 2009; Tape et al., 2018; van den Ende & Ampuero, 2020). Laboratory experiments have reported a range of precursors before earthquake-like lab-quakes (Bolton et al., 2019; Goebel et al., 2013; Johnson et al., 2013;

Marone, 1998; McLaskey & Lockner, 2014; Tinti et al., 2016). For example, direct observations of multi-scale damage evolution in the failure zone (fault zone) suggest that there are fault nucleation and propagation processes, but the evolution depends on the fault stress/strength condition, and can cause different precursors or precursors of different amplitudes for different fault systems (Renard et al., 2017, 2018). These experiments show similar variabilities of foreshock occurrence and properties in nature (X. Chen & Shearer, 2013; Trugman & Ross, 2019). However, it is difficult to directly compare conventional foreshocks with laboratory experiments because of their vastly different spatiotemporal scales. Often, foreshocks are examined in a much larger spatiotemporal scale than that of the earthquake nucleation scale, leaving their relation with the mainshocks less clear.

Another type of precursors are termed nucleation phases (Ellsworth & Beroza, 1995; McLaskey, 2019; Spudich & Cranswick, 1984). Specifically, the nucleation phases are defined as accelerating aseismic slip events that are responsible for the following earthquakes (Beroza & Ellsworth, 1996; Ellsworth & Beroza, 1995; Kato et al., 2012; Lapusta & Rice, 2003; Ruiz et al., 2014). These nucleation phase investigations can be theorized as the pre-slip model (Dodge et al., 1996; Ellsworth & Beroza, 1995; McLaskey, 2019). In this model, earthquakes are nucleated by propagating aseismic slips and foreshocks are just by-products of the mainshock nucleation process. This implies that small and large earthquakes are fundamentally different and the aseismic slip size determines the nucleation length, which scales with the final earthquake magnitude (Ellsworth & Beroza, 1995; Kato et al., 2012; Ruiz et al., 2014, 2017). Alternatively, numerous studies suggest that small and large earthquakes start the same way and it is difficult to predict the eventual earthquake magnitude or how the rupture would evolve based on the foreshocks or the P-wave onsets (Ide, 2019; Kilb et al., 2000; Meier et al., 2017; Okuda & Ide, 2018; Uchide & Ide, 2010; Yoon et al., 2019). These observations hint that small earthquakes can directly trigger other earthquakes by transferring stress and eventually leading to the mainshock when the stress or strength condition is favorable for continuous rupture propagation, the cascade model (Ide & Aochi, 2005; McLaskey, 2019; Lui & Lapusta, 2016).

One direction to improve the clarity of the problem lies in robust observations of immediate foreshocks for earthquakes spanning a large range of magnitude but occurring in the same fault system. The immediate foreshocks are microearthquakes shortly preceding the earthquakes and understanding these foreshocks will lead to improved understanding of the earthquake nucleation process. High-quality observations in such a relatively homogeneous geological environment are essential to track the effects of immediate foreshocks on the later-stage ruptures. In this study, we define immediate foreshocks as slip events that can generate highly similar P waves (herein we use preceding signals to denote the P waves of the immediate foreshocks) as those of the mainshocks and are within a few folds of the mainshock rupture dimension. We further require the immediate foreshocks to occur within 100 s to ensure that the earthquakes are near-instantaneous responses of the immediate foreshocks. We systematically investigate such immediate foreshocks for 13,895 $0.5 \leq M \leq 5.4$ Ridgecrest earthquakes from July 7, 2019 to August 6, 2019 that were reported in Southern California Earthquake Data Center (SCEDC; Hutton et al., 2010). We find 527 earthquakes with clear preceding signals of their P waves generated by the immediate foreshocks and these earthquakes are uniformly distributed across the whole fault system. These immediate foreshocks provide field observations that may bridge the conventional foreshocks and the laboratory foreshocks.

2. July 6, 2019 M_w 5.4 Ridgecrest Earthquake

The 2019 Ridgecrest earthquake sequence, including a M_w 6.4 foreshock and a M_w 7.1 mainshock, provides an excellent opportunity to investigate the earthquake nucleation process (Figure 1a). The earthquake sequence was well recorded by regional broadband seismic networks and a number of rapid response campaign deployments soon after the foreshock on July 4, 2019 (Cochran et al., 2020; Ross et al., 2019). In particular, multiple three-component nodal arrays (deployed after July 7, 2019 for a month) enable investigations of moderate to small magnitude earthquakes in detail (Catchings et al., 2020). In total, 13,895 earthquakes with magnitudes (M) ranging from 0.5 to 5.4 have been detected and located for the sequence (SCEDC; Hutton et al., 2010) during the deployment of the nodal array. SCEDC uses a few different magnitude scales, including moment magnitudes for larger events and local magnitudes for smaller events. The rich data set offers an ideal natural laboratory to examine the spatiotemporal evolution of a complete earthquake sequence at an unprecedented resolution (Cochran et al., 2020; Huang et al., 2020).
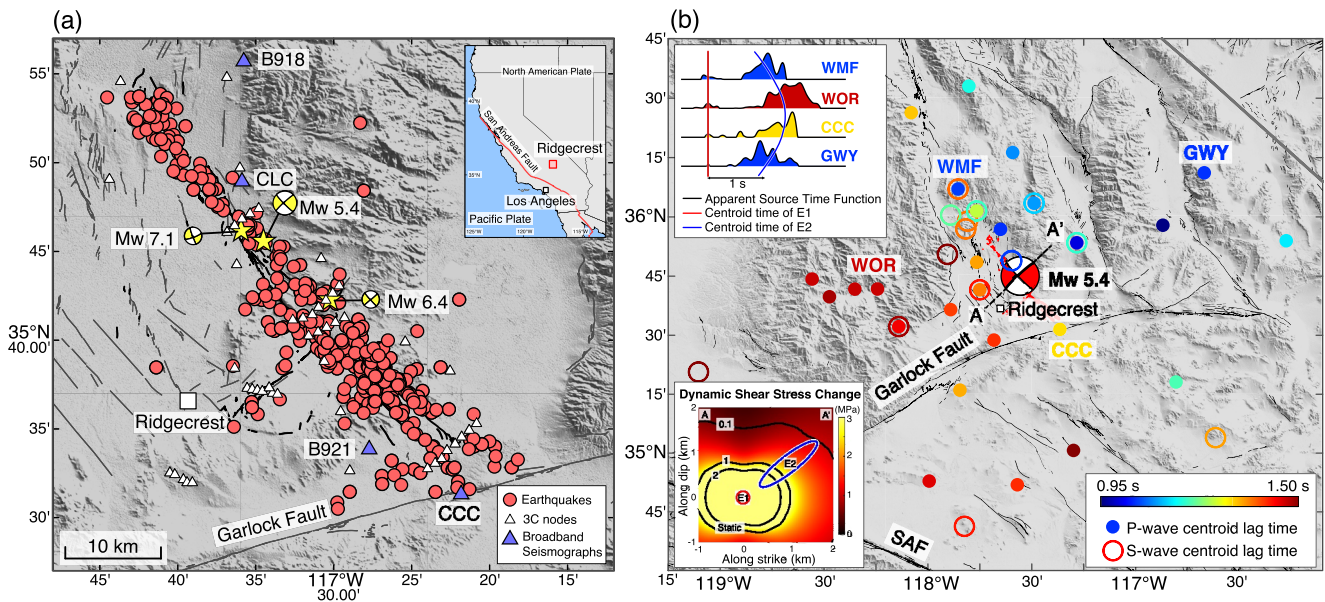
Figure 1. (a) Earthquakes with immediate foreshocks. White triangles are the nodal stations (Catchings et al., 2020) and blue triangles are four broadband seismographs (Caltech.Dataset, 2013). Fault traces are identified from geodetic observations (Jin & Fialko, 2020). The inset shows a regional map of California. (b) The centroid lag time distribution of the two subevents of the M_w 5.4 earthquake. The earthquake rupture propagated towards the northeast direction, perpendicular to the M_w 7.1 earthquake fault strike. The top-left inset shows four example apparent source time functions of the M_w 5.4 earthquake at different azimuths. The bottom left inset shows the stress perturbations at the subevent E2 from the subevent E1 (Figure S2). The color and contour show the peak dynamic- and static-stress perturbations respectively.

Located in between the foreshock and the mainshock, a July 6, 2019 M_w 5.4 earthquake has a clear immediate foreshock (referred to as E1 in Figures 1b, S1, and S2). The seismic records are band-pass filtered at 0.5–20.0 Hz with a causal 2nd-order Butterworth filter to avoid possible artifacts. There are preceding signals arriving at stations 0.8–1.2 s prior to the P waves, but they are 20 times smaller in amplitude on average. These signals share high resemblance with the P waves, and the onsets of both phases can be fit by scaling the records of a M 3.7 earthquake that is 1.5 km away from the hypocenter (SCEDC catalog; Hutton et al., 2010). We further implement the records of the M 3.7 earthquake as empirical Green's functions (eGfs) to remove the path effects to obtain apparent source time functions (ASTFs) of the M_w 5.4 earthquake for both P and S waves (Fan & McGuire, 2018; McGuire, 2004; Meng et al., 2020). The ASTFs show that there are at least two distinct subevents constituting the M_w 5.4 earthquake: the first subevent (E1) as the immediate foreshock releasing about 4.8% of the total seismic moment (equivalent to a M_w 4.5 earthquake), while the second subevent (E2) occurred about 0.8 s later and released the remaining moment (Figures 1b and S2).

To test the robustness of the immediate foreshock (subevent E1), we taper the ASTFs of E1 to zero (Figure S2a) and compute synthetic seismograms with only ASTFs of E2. The synthetics cannot explain the waveforms before the P-wave arrivals (Figure S2d), confirming the immediate foreshock. The ASTFs also show that the earthquake ruptured towards the northeast direction and the centroid locations of the two subevents are 1.1 km apart (Figure S3). With a second moments analysis (McGuire, 2017; Meng et al., 2020, Text S1), we find that the subevent E2 likely ruptured 1.3 and 1.0 km along the strike and dip directions, respectively. We further compute the strain-tensor perturbations on the fault plane generated by E1 by calculating the numerical spatial derivatives of the displacement field, with which we then use Hooke's law to obtain the stress perturbations (Text S1). The subevent E2 is situated in a region where both static and dynamic stress perturbations from the immediate foreshock exceed 0.1 MPa (Figure 1b), promoting an instantaneous slip event in the area (Figure S3). Our source model shows an evolving rupture process that the immediate foreshock cascadingly nucleated the sequential stage rupture, E2, through a stress-triggering process. This confirms our interpretation that E1 is causally related to E2.

3. Immediate Foreshocks

To understand the prevalence of such a nucleation process, we systematically investigate immediate foreshocks of other earthquakes of the 2019 Ridgecrest sequence. We find that similar seismic preceding signals are a common feature of 527 Ridgecrest earthquakes, indicating immediate foreshocks (Figure 1a). For example, similar immediate foreshocks are observed for a M 3.9 earthquake that is 2.7 km away from the M_w 5.4 event, and the P waves of the M 3.9 earthquake are almost identical to the P-wave onsets of the M_w 5.4 subevents (Figure 2). Further, clear immediate foreshocks can be identified for earthquakes as small as M 0.9 (Figure 2). We observe diverse immediate foreshocks of earthquakes spanning five magnitudes in a single 40-km-long fault system (Figures 1a and 3).

We identify these preceding signals by autocorrelating 0.5–1.0 s long P waves with vertical waveforms that precede the P waves by 100 s. The autocorrelation is independently performed for all stations within 30 km of the event epicenter (Text S2). For example, a preceding signal (indicating an immediate foreshock) is detected for a $M \leq 3.5$ earthquake when the average autocorrelation coefficient exceeds 0.8 for more than 10 stations and these stations are from a minimum azimuthal range of 180°. We do not perform the analysis on S-waves because they may be buried in the mainshock P waves, which may cause inconsistency in our detection procedure. For a detected immediate foreshock, we document the amplitude ratios and the preceding times (differential time from the autocorrelation procedure) between the preceding signals and the P waves (Figure 2 and see Text S2). The immediate foreshock is further examined by requiring the measured preceding time distribution to have a standard deviation that is less than 0.01 s for $M \leq 3.5$ earthquakes (Text S2). This quality control procedure assures that the immediate foreshocks generating the preceding signals are adjacent to their mainshocks and they share the same focal mechanisms, although the rupture details remain unresolved due to the data limitation. Finally, our procedure rules out the possibility of the detected preceding signals as the fault zone head waves because of a lack of systematic phase move-outs for sensors across the fault zone (Figures S4 and S5) (Ben-Zion & Malin, 1991; Ben-Zion et al., 1992).

In total, we examine 13,895 $0.5 \leq M \leq 5.4$ earthquakes in the Ridgecrest region that are reported in the SCEDC catalog (Hutton et al., 2010) and find that 527 events with immediate foreshocks that can be robustly identified (Table S1), out of which the M_w 5.4 earthquake preceded the M_w 7.1 earthquake while the remaining events were aftershocks of the M_w 7.1 earthquake. The lack of identifying immediate foreshocks with our procedure prior to the M_w 7.1 earthquake (July 6, 2019) is due to a data deficiency as the nodal arrays on the fault zone were only deployed after July 7, 2019 (Catchings et al., 2020). Our analysis relies on the near-fault data set and an autocorrelation method to study the earthquake preparation process. Therefore, we do not analyze the M_w 6.4 or M_w 7.1 earthquakes as the autocorrelation procedure is less effective for these large earthquakes, which would require other approaches for detailed analyses (e.g., Ellsworth & Bulut, 2018; Yoon et al., 2019).

We observe immediate foreshocks of earthquakes with magnitudes ranging from 0.9 to 5.4 and find these earthquakes have a similar magnitude-frequency distribution to that of the 13,895 investigated earthquakes (Figure S6). Additionally, the immediate foreshocks do not show characteristics that can differentiate the mainshocks of different fault segments (Figure 1a). These 527 earthquakes are distributed across the whole seismogenic zone from 0 to 13 km, penetrating beyond the creeping transition depth at 11.0 km (Figure 3g and see Text S3). The immediate foreshocks generate P waves preceding the mainshock P waves by 0.5–100 s. These preceding times do not seem to scale with earthquake magnitudes nor depths (Figures 3b and 3h). Intriguingly, amplitude ratios of $M \geq 2.5$ events are larger on average than those of smaller magnitude earthquakes (Figures 1a and S6c). However, the robustness of this observation is difficult to verify due to fewer $M \geq 2.5$ earthquakes (total 41 events). These $M \geq 2.5$ earthquakes are more likely to have higher amplitude ratios for the same noise level and detection threshold (detecting more low-amplitude preceding signals) because low amplitude preceding signals of smaller earthquakes are more likely buried in the background noise than those of larger events.

Using the differential times obtained from the autocorrelation procedure and a 1D average velocity model of Southern California (Lee et al., 2014), we further determine the relative locations between the 527 earthquakes and their immediate foreshocks (Figure 4a and see Text S4). About 84% of these immediate foreshocks are located within 0.2 km of the mainshock hypocenters with a median separation of 59 m
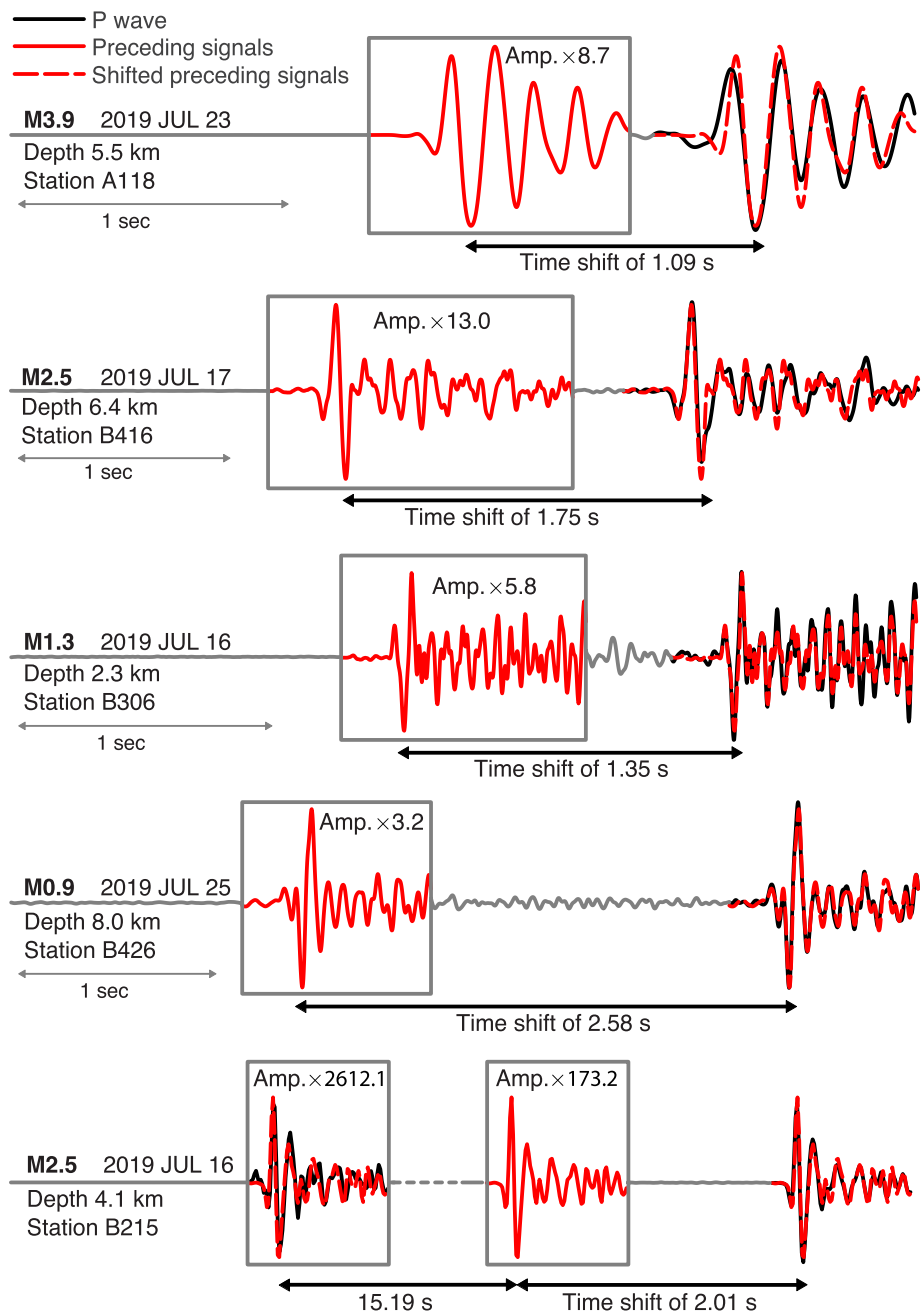
Figure 2. Example earthquake P waves and their preceding signals from the immediate foreshocks recorded by the nodal stations. The preceding signals are highlighted by the gray boxes and amplified for visual comparisons. The amplification factors are listed in the boxes. The records are the vertical components of example nodal array stations and the waveforms are band-pass filtered at 1–20 Hz with a casual 2nd-order Butterworth filter. The amplitude ratio and preceding time distributions for each event are shown in Figures S4 and S5.

(Figure 4a). We further evaluate the relative location uncertainty by performing jackknife resampling of the stations (Efron & Tibshirani, 1994) (Text S4). About 85% of the separation distance between the immediate foreshocks and mainshocks has a standard deviation less than 0.1 km with a median value of 15 m horizontally (Figure S7f). Vertically, 78% of the separation distance has a standard deviation less than 0.1 km with a median value of 31 m (Figure S7f). Further, we observe more than 85% of the immediate foreshocks occurred within 60 s of the mainshocks despite the searching window is 100 s long (Figure 4c). Without knowing the magnitudes and stress-drop estimates of the immediate foreshocks, we cannot evaluate the
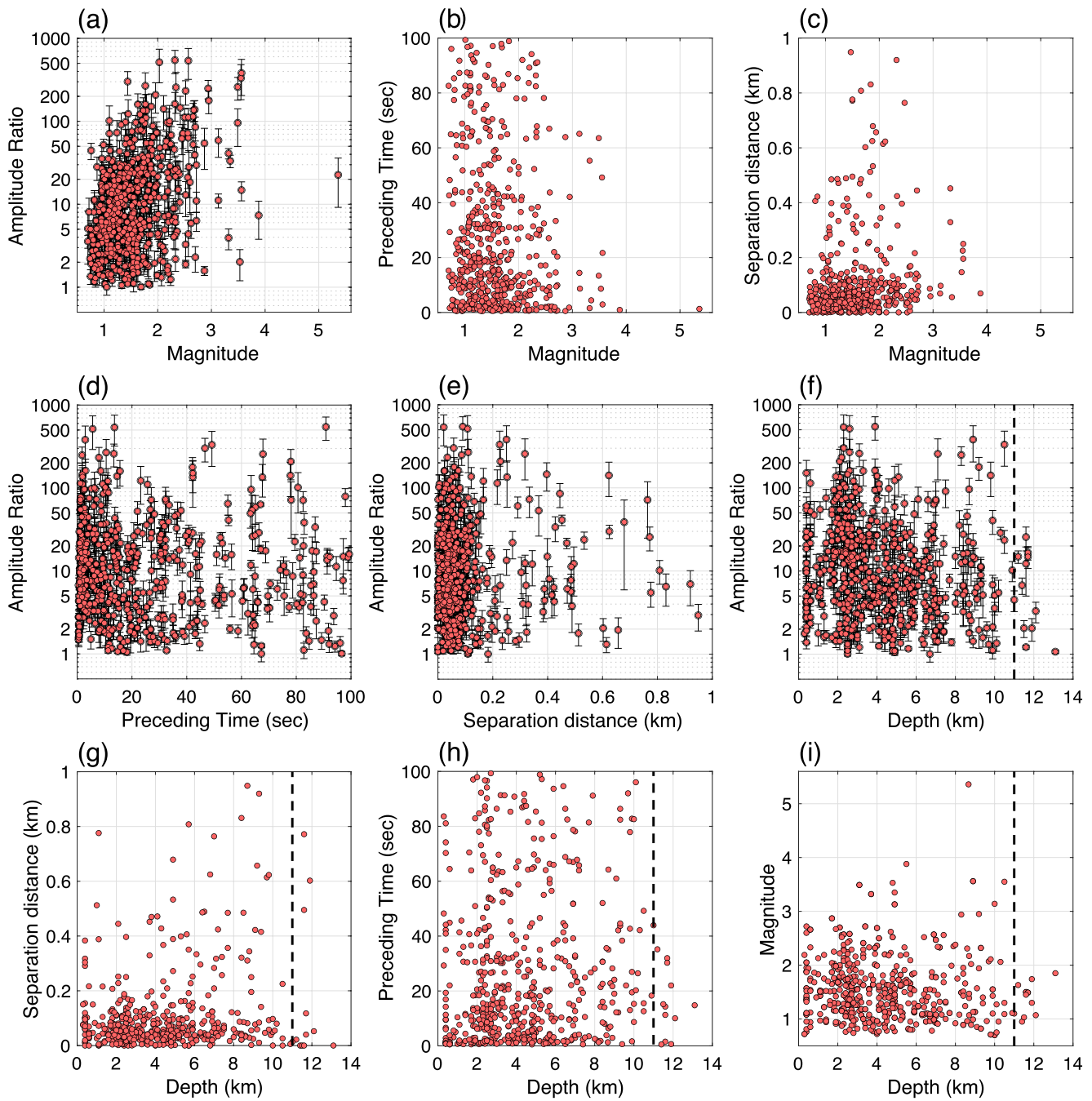
Figure 3. Scatter plots of the measured amplitude ratio, preceding time, magnitude, hypocentral separation, and depth of the earthquakes and their immediate foreshocks. The amplitude ratio error bar shows one standard deviation of the measurements for a given earthquake. The dashed line is the 95 percentile seismicity depth, 11.0 km (Text S3).

static/dynamic stress perturbations at the mainshock locations from the immediate foreshocks. However, the spatiotemporal clustering suggests that the immediate foreshocks likely near-instantaneously triggered the following slip, indicating a rapid rupture development (Shearer & Lin, 2009; Yoon et al., 2019).

Out of the 527 earthquakes, 48 earthquakes have series of successive preceding signals, indicating possible complex evolutions of the rupture developments. For example, we identify two immediate foreshocks for a *M* 2.5 earthquake (Figures 2 and S5). This sequence of preceding signals share high resemblances with the *M* 2.5 earthquake P waves with an average cross-correlation coefficient of 0.91, yet their amplitudes are
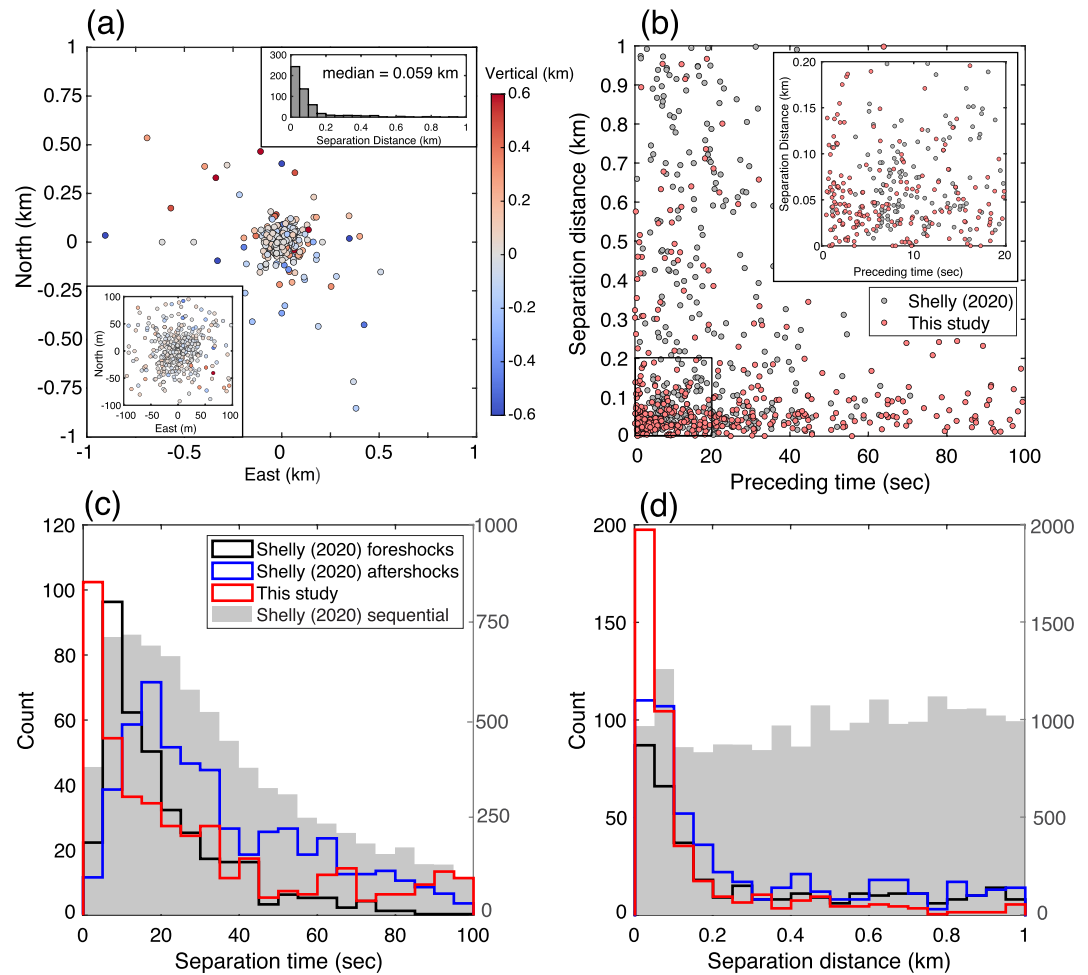
Figure 4. (a) Horizontal and vertical separations between the immediate foreshocks and the mainshocks. The bottom left insert shows the zoomed-in view of the hypocentral separations. The top right insert shows a histogram of the separation distances with a median of 0.059 km. (b) Preceding time and separation distance of the immediate foreshocks detected in this study and the selected foreshocks in a local high-resolution catalog (Shelly, 2020). The foreshocks are selected with preceding times less than 100 s and spatial separations less than 1 km of the mainshocks. (c and d) Distributions of separation time and distance to the mainshocks of the immediate foreshocks detected in this study and foreshocks/aftershocks in the Shelly, 2020 catalog. The foreshock and aftershock sequences are defined as two or more events occurring spatiotemporally within 100 s and 1 km, and the foreshock or aftershock magnitudes are smaller than those of the mainshocks. The gray histograms show the separation distance and time for sequential earthquake pairs in the Shelly, 2020 catalog within 1 km hypocentral distance of the 527 events with detected immediate foreshocks.

127.6 and 1067.8 times smaller than the P waves on average (Figure S5). These observations likely represent a hierarchical nucleation process that the observed earthquakes are products of a series of cascadingly triggered slip patches (Abercrombie & Mori, 1994; Ellsworth & Bulut, 2018; Fukao & Furumoto, 1985; Ide, 2019; Okuda & Ide, 2018; Wyss & Brune, 1967). These observations also suggest that the Ridgecrest fault system may have a fractal strength or stress structure over orders of scale. Characteristics of these 48 earthquakes and their immediate foreshocks, including the earthquake location, amplitude ratio, and preceding time, show no differences to those of the rest 479 earthquakes that only have single immediate foreshocks, rendering that earthquake rupture development is stochastic and local fine-scale heterogeneous fault properties control the rupture evolution (Ide, 2019; Ide & Aochi, 2005; McLaskey, 2019; Trugman, McBrearty, et al., 2020).

4. Discussions and Conclusions

The observed immediate foreshocks show clear spatiotemporal correlations with the following earthquakes (Figures 4a and 4b), but are they precursors of the earthquakes or simply random forerunners? To evaluate the influence of the immediate foreshocks in nucleating the following slip, we compare the immediate foreshocks with cataloged earthquakes in Shelly (2020). We first investigate the spatiotemporal behaviors of all the cataloged earthquakes that are within 1 km to the 527 earthquake hypocenters, which have one or more immediate foreshocks. The separation distance and time between two sequential cataloged earthquakes show different distributions comparing to those of the immediate foreshocks (Figures 4c and 4d). These sequential earthquakes seem to be relatively uniformly separated in space (within 1 km), and the separation time seems to be Poissonian. Such characteristics show that sequential earthquakes are mostly independent, random cases. In contrast, the immediate foreshocks cluster in space and time, suggesting they are not random but more likely have influenced the following earthquakes, hence causally related to the mainshocks.

We also compare the immediate foreshocks with correlated seismicity in Shelly (2020), including foreshock-mainshock and mainshock-aftershock sequences (Figure S8). These sequences are defined as sequential earthquakes occurring within 1 km and 100 s and the foreshocks/aftershocks having smaller magnitudes comparing to the mainshocks (across the whole Ridgecrest region, not just near the 527 earthquakes with immediate foreshocks). In Shelly (2020), there are 363 foreshock-mainshock and 519 mainshock-aftershock sequences (Text S5). The separation distances between the foreshocks/aftershocks and the mainshocks show similarities with the immediate foreshocks as they all cluster within 0.2 km of the mainshock hypocenters (Figure 4d). The separation time distributions are different (Figure 4c). There seems to be an apparent paucity of aftershocks soon after the mainshocks in the Shelly (2020) catalog and most of the aftershocks seem to occur at or after 20 s of the mainshocks. The lack of aftershocks soon after the mainshocks may be due to the high-amplitude coda waves or noises in the records (Kagan & Houston, 2005). The foreshocks in the high-resolution catalog are akin to the immediate foreshocks, that is, clustering spatiotemporally with the mainshocks, but also show differences. Most of the foreshocks occurred more than 5 s ahead of the mainshocks, while our immediate foreshocks peak within 5 s of the following mainshocks (Figures 4b and 4c). Further, the occurrence of the 527 observed immediate foreshocks and the 363 foreshocks in Shelly (2020) follow the inverse Omori's law as there are more immediate foreshocks and catalog foreshocks as the mainshocks approach, but the two classes of seismicity grow at different rates (Figure S9 and see Text S6). As the completeness of our detection for immediate foreshocks is unclear, we caution direct interpretation of the growing rate, but simply take this as a line of evidence that both our detected immediate foreshocks and the foreshocks in Shelly (2020) are causally related to the mainshocks (Cattania & Segall, 2021).

In most studies, the term "foreshock" is loosely defined, and they are often considered in much larger spatiotemporal scales, that is, over tens of kilometers and/or days of periods (Abercrombie & Mori, 1996; X. Chen & Shearer, 2013; Moutote et al., 2021; Shearer & Lin, 2009; Trugman & Ross, 2019; van den Ende & Ampuero, 2020). The foreshocks that we search in the high-resolution catalog (Shelly, 2020) are specific events analogous to our immediate foreshocks, and they are selected based on strict constraints in space and time (Figure 4). Therefore, the observed variations of the foreshocks and immediate foreshocks in Figure 4c may not be inconsistent but represent the same process at two resolutions. For example, characteristics of these foreshock-mainshock sequences in Shelly (2020) show similar patterns as those of the observed immediate foreshocks, and we do not find clear scaling relationships among the earthquake magnitude, depth, preceding time, and magnitude difference (Figure S8). Therefore, the foreshocks in the high-resolution catalog (Shelly, 2020) and the immediate foreshocks in this study may demonstrate the same type of preparation phase for the mainshocks. Particularly, our immediate foreshocks offer a high-resolution view of slip events ahead of the earthquake onsets because of the spatial collocation and the short separation time. They demonstrate a near-instantaneous response of the following slip events, indicating that the mainshocks are nucleated by stress transferring from the immediate foreshocks.

The current set of observations can be best interpreted as representations of the cascade model (Aochi & Ide, 2004; Fukao & Furumoto, 1985; Ide & Aochi, 2005; Lui & Lapusta, 2016; Wyss & Brune, 1967). In this cascade model, a slip event on a small fault patch that is adjacent or within the earthquake rupture area

rapidly transfers stress to a surrounding fault and leads to an unsteady dynamic rupture (Ide & Aochi, 2005; Lui & Lapusta, 2016; McLaskey, 2019). Such processes have been observed in earthquakes with a range of magnitudes. For example, the 1964 M_w 9.2 Alaska earthquake was shortly preceded by a sequence of earthquakes within 100 s (likely immediate foreshocks) before its onset, and the propagating rupture of the sequence eventually led to the great earthquake (Wyss & Brune, 1967). The propagation of such a cascade process is controlled by the local stress and strength heterogeneities, which effectively reflect as hierarchically distributed fault patches, and naturally, the barriers between such patches determine the termination of the cascade process, the earthquake eventual magnitude (Aochi & Ide, 2004; Fukao & Furumoto, 1985; Ide & Aochi, 2005; Noda et al., 2013). It is worth noting that large earthquakes (e.g., M ≥ 6) have P waves significantly different from those of small events, therefore, we did not investigate the M_w 6.4 and the M_w 7.1 Ridgecrest earthquakes. However, foreshocks seem to have cascadingly triggered the M_w 6.4 earthquake without evidence of observable aseismic slips (K. Chen et al., 2020; Ellsworth et al., 2020; Huang et al., 2020; Ross et al., 2019; Wang et al., 2020; Yue et al., 2021).

The structure of hierarchical fault patches implies multiscale heterogeneities, which is likely the physical cause of the series of successive preceding signals (Figures 2 and S5). These fault patches and heterogeneities associate with the stress distribution, fault roughness, and fault gouge, which may have developed naturally as the fault structure evolves over multiple seismic cycles (Andrews, 1980; Davidesko et al., 2014; Mai & Beroza, 2000; Martel et al., 1988; Trugman, Ross, & Johnson, 2020). In particular, the 2019 M_w 7.1 Ridgecrest earthquake has caused stress variabilities on length scales of hundreds of meters or less, leading to faulting complexities throughout the earthquake sequence (Trugman, Ross, & Johnson, 2020). Such complex structures and heterogeneities have scales comparable to those of the separation distances between the immediate foreshocks and mainshocks (Figure 4), favoring the cascade nucleation process. Previous numerical studies show that the rate-and-state friction law and a set of randomly distributed fractal fault patches can produce a wide variety of cascading rupture scenarios for both small and large earthquakes (Fukao & Furumoto, 1985; Ide, 2019). Furthermore, recent laboratory experiments suggest a rate-dependent cascade process that may have been facilitated by the varying nucleation length in addition to the fault property heterogeneities (McLaskey, 2019). These studies suggest that the final magnitude is the only difference between small and large earthquakes. For the Ridgecrest earthquakes, the lack of scaling relations between the preceding signals and the P waves and the diverse characteristics of the immediate foreshocks indicate such a stochastic rupture development and support the cascade model (Figure 3). Our results concur that earthquakes nucleate in a similar fashion and large events are simply results of favorable continuous rupture conditions. For example, the M 3.9 and the M_w 5.4 earthquakes occurred within 2.6 km and have similar preceding signals (SCEDC; Hutton et al., 2010), but the final moments were 165 times different (Figures 2, S1–S2, and S4). Such disparities emphasize that fine-scale heterogeneities or barriers modulate earthquake rupture developments in complex ways.

Another possible nucleation mechanism is the preslip model (Dodge et al., 1996; Ellsworth & Beroza, 1995; McLaskey, 2019). In this model, the final earthquake magnitude correlates with the aseismic slip size, which can trigger foreshocks but the foreshocks do not prepare the following mainshocks. Therefore, this model hints that the aseismic nucleation characteristics would affect the later stage rupture of an earthquake, although seismic observations of the preslip model may be indistinguishable from those caused by the cascade model (Ellsworth & Beroza, 1995). Recent observations of some large subduction zone earthquakes can be explained by this model (Kato et al., 2012; Ruiz et al., 2014, 2017). The preslip model would suggest a coalescence of seismicity migrating around the earthquake epicenter for some extended period before the fault slip reaching a critical nucleation length (Lapusta & Rice, 2003; Tape et al., 2018). In our observations, earthquakes with immediate foreshocks occurred at all depths beyond the transition zone, and we rarely observe more than one preceding signal for a given earthquake. However, additional preceding signals may have been missed by our autocorrelation procedure, which is less effective at detecting aseismic slips or slip events that are away from the earthquake hypocenter. It is possible that multiple processes have occurred concurrently and have modulated the nucleation process as a rate-dependent feedback system, which has been documented in experiments, simulations, and field observations (Cattania & Segall, 2021; McLaskey, 2019; Lapusta & Rice, 2003; Yao et al., 2020).

We do not observe seismic preceding signals for every investigated earthquake. Roughly, 4% of the 13,895 earthquakes have identifiable immediate foreshocks despite we find immediate foreshocks for events with magnitudes spanning from 0.9 to 5.4. This is likely limited by the data as the majority of the immediate foreshocks are inferred from the nodal array data, and the preceding signals are often buried in the noise at the regional network stations. It is also possible that there are more immediate foreshocks but their separation times are too short to be resolved by our current procedure or available data. Additionally, our procedure may have excluded seismic preceding signals beyond the 100 s time window that we have scanned through. In this case, there might be other preparation processes than the near-instantaneous stress transferring nucleation as demonstrated by the immediate foreshocks. Finally, our observations represent one class of the earthquake nucleation processes and there are other possible physical mechanisms initiating the Ridgecrest earthquakes in addition to the aforementioned end-member models. Nevertheless, the immediate foreshocks highlight the importance of near-field observations, in particular, the needs of fault-zone observations.

Whether the growth trajectory of an earthquake can be robustly forecasted in real-time depends on understanding the influences of the earthquake foreshocks over the later stage rupture (Iio, 1992; McLaskey, 2019; Meier et al., 2017; Mori & Kanamori, 1996). Fine-scale rate-dependent physical processes, for example, grain crushing, microcracking, and plastic deformation, may have strong impacts on the earthquake rupture development (Yamashita, 2000; Xu et al., 2019). Such processes are challenging to measure geophysically and cannot be deterministically predicted, which may cause small and large earthquakes showing similar developing processes.

For the Ridgecrest earthquakes, we find immediate foreshocks for 527 earthquakes with magnitudes from 0.9 to 5.4 that may have helped to nucleate the earthquakes. Numerous earthquakes occurred in the same region showing similar seismic preceding signals but developed into events with different eventual magnitudes, illuminating the limited predictability of the earthquake growth process (Figure 3). For instance, we find that there is no scaling relationship between the amplitude ratio or the preceding time with the earthquake magnitude (Figures 3a and 3b). However, we find that all the observed immediate foreshocks occurred within 100 s of the earthquakes with a temporal clustering around 7 s and 0.06 km (Figure S10). This time-distance clustering of the 527 earthquakes and their immediate foreshocks shows a possible common preparation process for both small and large events that nucleate earthquakes near-instantaneously in the Ridgecrest fault system.

Data Availability Statement

The 13,895 earthquakes investigated in the study are from the Southern California Earthquake Data Center catalog (SCEDC; Hutton et al., 2010). The high-resolution catalog used for comparison is from Shelly (2020). The seismic records were provided by the Data Management Center (DMC) of the Incorporated Research Institutions for Seismology (IRIS) and the SCEDC (Caltech.Dataset, 2013). The nodal array data is openly available through IRIS DMC and was acquired by the U.S. Geological Survey (USGS) (Catchings et al., 2020), the Southern California Earthquake Center (SCEC), and SCEC member institutions. The 1D velocity model used in this study is obtained from averaging the community velocity model of Southern California (Lee et al., 2014). The earthquakes that have immediate foreshocks are listed in Table S1 and can be obtained at Mendeley Data repository (https://data.mendeley.com/datasets/n3mkf9mpd2/1).

References

Abercrombie, R. E., & Mori, J. (1994). Local observations of the onset of a large earthquake: 28 June 1992 Landers, California. *Bulletin of the Seismological Society of America*, *84*(3), 725–734. https://doi.org/10.1785/bssa0840030497

Abercrombie, R. E., & Mori, J. (1996). Occurrence patterns of foreshocks to large earthquakes in the western United States. *Nature*, *381*(6580), 303–307. https://doi.org/10.1038/381303a0

Andrews, D. (1980). A stochastic fault model: 1. static case. *Journal of Geophysical Research*, *85*(B7), 3867–3877. https://doi.org/10.1029/jb085ib07p03867

Aochi, H., & Ide, S. (2004). Numerical study on multi-scaling earthquake rupture. *Geophysical Research Letters*, *31*(2), L02606. https://doi.org/10.1029/2003gl018708

Ben-Zion, Y., Katz, S., & Leary, P. (1992). Joint inversion of fault zone head waves and direct P arrivals for crustal structure near major faults. *Journal of Geophysical Research*, *97*(B2), 1943–1951. https://doi.org/10.1029/91jb02748

Ben-Zion, Y., & Malin, P. (1991). San Andreas Fault zone head waves near Parkfield, California. *Science*, *251*(5001), 1592–1594. https://doi.org/10.1126/science.251.5001.1592

Beroza, G. C., & Ellsworth, W. L. (1996). Properties of the seismic nucleation phase. *Tectonophysics*, *261*(1–3), 209–227. https://doi.org/10.1016/0040-1951(96)00067-4

Bolton, D. C., Shokouhi, P., Rouet-Leduc, B., Hulbert, C., Rivière, J., Marone, C., & Johnson, P. A. (2019). Characterizing acoustic signals and searching for precursors during the laboratory seismic cycle using unsupervised machine learning. *Seismological Research Letters*, *90*(3), 1088–1098. https://doi.org/10.1785/0220180367

Bouchon, M., Durand, V., Marsan, D., Karabulut, H., & Schmittbuhl, J. (2013). The long precursory phase of most large interplate earthquakes. *Nature Geoscience*, *6*(4), 299–302. https://doi.org/10.1038/ngeo1770

Caltech. Dataset (2013). Southern California Earthquake Data Center. https://doi.org/10.7909/C3WD3xH1

Catchings, R. D., Goldman, M., Steidl, J., Chan, J., Allam, A., Criley, C., et al. (2020). Nodal seismograph recordings of the 2019 Ridgecrest earthquake sequence. *Seismological Research Letters*, *91*(6), 3622–3633. https://doi.org/10.1785/0220200203

Cattania, C., & Segall, P. (2021). Precursory slow slip and foreshocks on rough faults. *Journal of Geophysical Research: Solid Earth*, *126*(4), e2020JB020430. https://doi.org/10.1029/2020jb020430

Chen, K., Avouac, J.-P., Aati, S., Milliner, C., Zheng, F., & Shi, C. (2020). Cascading and pulse-like ruptures during the 2019 Ridgecrest earthquakes in the eastern California shear zone. *Nature Communications*, *11*(1), 1–8. https://doi.org/10.1038/s41467-019-13750-w

Chen, X., & Shearer, P. M. (2013). California foreshock sequences suggest aseismic triggering process. *Geophysical Research Letters*, *40*(11), 2602–2607. https://doi.org/10.1002/grl.50444

Cochran, E. S., Wolin, E., McNamara, D. E., Yong, A., Wilson, D., Alvarez, M., et al. (2020). The U.S. Geological Survey's rapid seismic array deployment for the 2019 Ridgecrest Earthquake Sequence. *Seismological Research Letters*, *91*(4), 1952–1960. https://doi.org/10.1785/0220190296

Dascher-Cousineau, K., Lay, T., & Brodsky, E. E. (2020). Two foreshock sequences post gulia and wiemer (2019). *Seismological Society of America*, *91*(5), 2843–2850. https://doi.org/10.1785/0220200082

Davidesko, G., Sagy, A., & Hatzor, Y. H. (2014). Evolution of slip surface roughness through shear. *Geophysical Research Letters*, *41*(5), 1492–1498. https://doi.org/10.1002/2013gl058913

Dodge, D. A., Beroza, G. C., & Ellsworth, W. L. (1996). Detailed observations of California foreshock sequences: Implications for the earthquake initiation process. *Journal of Geophysical Research*, *101*(B10), 22371–22392. https://doi.org/10.1029/96jb02269

Efron, B., & Tibshirani, R. J. (1994). *An introduction to the bootstrap*. CRC press.

Ellsworth, W. L., Barbour, A. J., & Shelly, D. R. (2020). *Foreshock cascade to failure in the m_w 6.4 July 4, 2019 Ridgecrest, California earthquake*. Poster Presentation at 2020 SCEC Annual Meeting.

Ellsworth, W. L., & Beroza, G. (1995). Seismic evidence for an earthquake nucleation phase. *Science*, *268*(5212), 851–855. https://doi.org/10.1126/science.268.5212.851

Ellsworth, W. L., & Bulut, F. (2018). Nucleation of the 1999 Izmit earthquake by a triggered cascade of foreshocks. *Nature Geoscience*, *11*(7), 531–535. https://doi.org/10.1038/s41561-018-0145-1

Fan, W., & McGuire, J. J. (2018). Investigating microearthquake finite source attributes with IRIS community wavefield demonstration experiment in Oklahoma. *Geophysical Journal International*, *214*(2), 1072–1087. https://doi.org/10.1093/gji/ggy203

Fukao, Y., & Furumoto, M. (1985). Hierarchy in earthquake size distribution. *Physics of the Earth and Planetary Interiors*, *37*(2–3), 149–168. https://doi.org/10.1016/0031-9201(85)90048-2

Goebel, T., Schorlemmer, D., Becker, T., Dresen, G., & Sammis, C. (2013). Acoustic emissions document stress changes over many seismic cycles in stick-slip experiments. *Geophysical Research Letters*, *40*(10), 2049–2054. https://doi.org/10.1002/grl.50507

Gulia, L., & Wiemer, S. (2019). Real-time discrimination of earthquake foreshocks and aftershocks. *Nature*, *574*(7777), 193–199. https://doi.org/10.1038/s41586-019-1606-4

Huang, H., Meng, L., Bürgmann, R., Wang, W., & Wang, K. (2020). Spatio-temporal foreshock evolution of the 2019 M 6.4 and M 7.1 Ridgecrest, California earthquakes. *Earth and Planetary Science Letters*, *551*, 116582. https://doi.org/10.1016/j.epsl.2020.116582

Hutton, K., Woessner, J., & Hauksson, E. (2010). Earthquake monitoring in southern California for seventy-seven years (1932–2008). *Bulletin of the Seismological Society of America*, *100*(2), 423–446. https://doi.org/10.1785/0120090130

Ide, S. (2019). Frequent observations of identical onsets of large and small earthquakes. *Nature*, *573*(7772), 112–116. https://doi.org/10.1038/s41586-019-1508-5

Ide, S., & Aochi, H. (2005). Earthquakes as multiscale dynamic ruptures with heterogeneous fracture surface energy. *Journal of Geophysical Research*, *110*(B11), B11303. https://doi.org/10.1029/2004jb003591

Iio, Y. (1992). Slow initial phase of the P-wave velocity pulse generated by microearthquakes. *Geophysical Research Letters*, *19*(5), 477–480. https://doi.org/10.1029/92gl00179

Jin, Z., & Fialko, Y. (2020). Finite slip models of the 2019 Ridgecrest earthquake sequence constrained by space geodetic data and aftershock locations. *Bulletin of the Seismological Society of America*, *110*(4), 1660–1679. https://doi.org/10.1785/0120200060

Johnson, P. A., Ferdowsi, B., Kaproth, B. M., Scuderi, M., Griffa, M., Carmeliet, J., et al. (2013). Acoustic emission and microslip precursors to stick-slip failure in sheared granular material. *Geophysical Research Letters*, *40*(21), 5627–5631. https://doi.org/10.1002/2013gl057848

Kagan, Y. Y., & Houston, H. (2005). Relation between mainshock rupture process and Omari's law for aftershock moment release rate. *Geophysical Journal International*, *163*(3), 1039–1048. https://doi.org/10.1111/j.1365-246x.2005.02772.x

Kanamori, H. (2003). Earthquake prediction: An overview. *International Geophysics*, *81*, 1205–1216. https://doi.org/10.1016/S0074-6142(03)80186-9

Kanamori, H., & Cipar, J. J. (1974). Focal process of the great Chilean earthquake May 22, 1960. *Physics of the Earth and Planetary Interiors*, *9*(2), 128–136. https://doi.org/10.1016/0031-9201(74)90029-6

Kato, A., Obara, K., Igarashi, T., Tsuruoka, H., Nakagawa, S., & Hirata, N. (2012). Propagation of slow slip leading up to the 2011 Mw 9.0 Tohoku-Oki earthquake. *Science*, *335*(6069), 705–708. https://doi.org/10.1126/science.1215141

Kilb, D., Gomberg, J., & Bodin, P. (2000). Triggering of earthquake aftershocks by dynamic stresses. *Nature*, *408*(6812), 570–574. https://doi.org/10.1038/35046046

Lapusta, N., & Rice, J. R. (2003). Nucleation and early seismic propagation of small and large events in a crustal earthquake model. *Journal of Geophysical Research*, *108*(B4), 2205. https://doi.org/10.1029/2001jb000793

Lee, E.-J., Chen, P., Jordan, T. H., Maechling, P. B., Denolle, M. A., & Beroza, G. C. (2014). Full-3-D tomography for crustal structure in southern California based on the scattering-integral and the adjoint-wavefield methods. *Journal of Geophysical Research: Solid Earth*, *119*(8), 6421–6451. https://doi.org/10.1002/2014jb011346

Liu, Y., McGuire, J. J., & Behn, M. D. (2020). Aseismic transient slip on the Gofar transform fault, East Pacific Rise. *Proceedings of the National Academy of Sciences of the United States of America*, *117*(19), 10188–10194. https://doi.org/10.1073/pnas.1913625117

Lui, S. K., & Lapusta, N. (2016). Repeating microearthquake sequences interact predominantly through postseismic slip. *Nature Communications*, *7*(1), 1–7. https://doi.org/10.1038/ncomms13020

Mai, P. M., & Beroza, G. C. (2000). Source scaling properties from finite-fault-rupture models. *Bulletin of the Seismological Society of America*, *90*(3), 604–615. https://doi.org/10.1785/0119990126

Marone, C. (1998). Laboratory-derived friction laws and their application to seismic faulting. *Annual Review of Earth and Planetary Sciences*, *26*(1), 643–696. https://doi.org/10.1146/annurev.earth.26.1.643

Martel, S. J., Pollard, D. D., & Segall, P. (1988). Development of simple strike-slip fault zones, Mount Abbot quadrangle, Sierra Nevada, California. *Geological Society of America Bulletin*, *100*(9), 1451–1465. https://doi.org/10.1130/0016-7606(1988)100<1451:dosssf>2.3.co;2

McGuire, J. J. (2004). Estimating finite source properties of small earthquake ruptures. *Bulletin of the Seismological Society of America*, *94*(2), 377–393. https://doi.org/10.1785/0120030091

McGuire, J. J. (2017). A MATLAB toolbox for estimating the second moments of earthquake ruptures. *Seismological Research Letters*, *88*(2A), 371–378. https://doi.org/10.1785/0220160170

McLaskey, G. C. (2019). Earthquake initiation from laboratory observations and implications for foreshocks. *Journal of Geophysical Research: Solid Earth*, *124*(12), 12882–12904. https://doi.org/10.1029/2019jb018363

McLaskey, G. C., & Lockner, D. A. (2014). Preslip and cascade processes initiating laboratory stick slip. *Journal of Geophysical Research: Solid Earth*, *119*(8), 6323–6336. https://doi.org/10.1002/2014jb011220

Mclaskey, G. C., & Yamashita, F. (2017). Slow and fast ruptures on a laboratory fault controlled by loading characteristics. *Journal of Geophysical Research: Solid Earth*, *122*(5), 3719–3738. https://doi.org/10.1002/2016jb013681

Meier, M.-A., Ampuero, J., & Heaton, T. H. (2017). The hidden simplicity of subduction megathrust earthquakes. *Science*, *357*(6357), 1277–1281. https://doi.org/10.1126/science.aan5643

Meng, H., McGuire, J. J., & Ben-Zion, Y. (2020). Semiautomated estimates of directivity and related source properties of small to moderate southern California earthquakes using second seismic moments. *Journal of Geophysical Research: Solid Earth*, *125*(4), e2019JB018566. https://doi.org/10.1029/2019jb018566

Mignan, A. (2012). Seismicity precursors to large earthquakes unified in a stress accumulation framework. *Geophysical Research Letters*, *39*(21), L21308. https://doi.org/10.1029/2012GL053946

Mignan, A. (2014). The debate on the prognostic value of earthquake foreshocks: A meta-analysis. *Scientific Reports*, *4*, 4099. https://doi.org/10.1038/srep04099

Mori, J., & Kanamori, H. (1996). Initial rupture of earthquakes in the 1995 Ridgecrest, California sequence. *Geophysical Research Letters*, *23*(18), 2437–2440. https://doi.org/10.1029/96gl02491

Moutote, L., Marsan, D., Lengliné, O., & Duputel, Z. (2020). *Low significance of foreshock activity in Southern California*.

Moutote, L., Marsan, D., Lengliné, O., & Duputel, Z. (2021). Rare occurrences of non-cascading foreshock activity in southern California. *Geophysical Research Letters*, *48*(7), e2020GL091757. https://doi.org/10.1029/2020gl091757

Noda, H., Nakatani, M., & Hori, T. (2013). Large nucleation before large earthquakes is sometimes skipped due to cascade-up implications from a rate and state simulation of faults with hierarchical asperities. *Journal of Geophysical Research: Solid Earth*, *118*(6), 2924–2952. https://doi.org/10.1002/jgrb.50211

Ohnaka, M. (1992). Earthquake source nucleation: A physical model for short-term precursors. *Tectonophysics*, *211*(1–4), 149–178. https://doi.org/10.1016/0040-1951(92)90057-d

Okuda, T., & Ide, S. (2018). Hierarchical rupture growth evidenced by the initial seismic waveforms. *Nature Communications*, *9*(1), 1–7. https://doi.org/10.1038/s41467-018-06168-3

Pritchard, M. E., Allen, R. M., Becker, T. W., Behn, M. D., Brodsky, E. E., Bürgmann, R., et al. (2020). New opportunities to study earthquake precursors. *Seismological Research Letters*, *91*(20), 2444–2447. https://doi.org/10.1785/0220200089

Renard, F., Cordonnier, B., Kobchenko, M., Kandula, N., Weiss, J., & Zhu, W. (2017). Microscale characterization of rupture nucleation unravels precursors to faulting in rocks. *Earth and Planetary Science Letters*, *476*, 69–78. https://doi.org/10.1016/j.epsl.2017.08.002

Renard, F., Weiss, J., Mathiesen, J., Ben-Zion, Y., Kandula, N., & Cordonnier, B. (2018). Critical evolution of damage toward system-size failure in crystalline rock. *Journal of Geophysical Research: Solid Earth*, *123*(2), 1969–1986. https://doi.org/10.1002/2017jb014964

Ross, Z. E., Idini, B., Jia, Z., Stephenson, O. L., Zhong, M., Wang, X., & Moore, A. W. (2019). Hierarchical interlocked orthogonal faulting in the 2019 Ridgecrest earthquake sequence. *Science*, *3665*, 346–351. https://doi.org/10.1126/science.aaz0109

Ruiz, S., Aden-Antoniow, F., Baez, J., Otarola, C., Potin, B., del Campo, F., et al. (2017). Nucleation phase and dynamic inversion of the Mw 6.9 Valparaíso 2017 earthquake in central Chile. *Geophysical Research Letters*, *44*(20), 10–290. https://doi.org/10.1002/2017gl075675

Ruiz, S., Metois, M., Fuenzalida, A., Ruiz, J., Leyton, F., Grandin, R., et al. (2014). Intense foreshocks and a slow slip event preceded the 2014 Iquique Mw 8.1 earthquake. *Science*, *345*(6201), 1165–1169. https://doi.org/10.1126/science.1256074

Seif, S., Zechar, J. D., Mignan, A., Nandan, S., & Wiemer, S. (2019). Foreshocks and their potential deviation from general seismicity. *Bulletin of the Seismological Society of America*, *109*(1), 1–18. https://doi.org/10.1785/0120170188

Shearer, P. M., & Lin, G. (2009). Evidence for Mogi doughnut behavior in seismicity preceding small earthquakes in Southern California. *Journal of Geophysical Research*, *114*(B1), B01318. https://doi.org/10.1029/2008jb005982

Shelly, D. R. (2020). A high-resolution seismic catalog for the initial 2019 Ridgecrest earthquake sequence: Foreshocks, aftershocks, and faulting complexity. *Seismological Research Letters*, *91*(4), 1971–1978. https://doi.org/10.1785/0220190309

Spudich, P., & Cranswick, E. (1984). Direct observation of rupture propagation during the 1979 Imperial Valley earthquake using a short baseline accelerometer array. *Bulletin of the Seismological Society of America*, *74*(6), 2083–2114. https://doi.org/10.1785/bssa0740062083

Sykes, L. R., Shaw, B. E., & Scholz, C. H. (1999). Rethinking earthquake prediction. *Pure and Applied Geophysics*, *155*(2–4), 207–232. https://doi.org/10.1007/s000240050263

Tape, C., Holtkamp, S., Silwal, V., Hawthorne, J., Kaneko, Y., Ampuero, J. P., et al. (2018). Earthquake nucleation and fault slip complexity in the lower crust of central Alaska. *Nature Geoscience*, *11*(7), 536–541. https://doi.org/10.1038/s41561-018-0144-2

Tinti, E., Scuderi, M., Scognamiglio, L., Di Stefano, G., Marone, C., & Collettini, C. (2016). On the evolution of elastic properties during laboratory stick-slip experiments spanning the transition from slow slip to dynamic rupture. *Journal of Geophysical Research: Solid Earth*, *121*(12), 8569–8594. https://doi.org/10.1002/2016jb013545

Trugman, D. T., McBrearty, I. W., Bolton, D. C., Guyer, R. A., Marone, C., & Johnson, P. A. (2020). The spatiotemporal evolution of granular microslip precursors to laboratory earthquakes. *Geophysical Research Letters*, *47*(16), e2020GL088404. https://doi.org/10.1029/2020gl088404

Trugman, D. T., & Ross, Z. E. (2019). Pervasive foreshock activity across Southern California. *Geophysical Research Letters*, *46*(15), 8772–8781. https://doi.org/10.1029/2019gl083725

Trugman, D. T., Ross, Z. E., & Johnson, P. A. (2020). Imaging stress and faulting complexity through earthquake waveform similarity. *Geophysical Research Letters*, *47*(1), e2019GL085888. https://doi.org/10.1029/2019gl085888

Uchide, T., & Ide, S. (2010). Scaling of earthquake rupture growth in the Parkfield area: Self-similar growth and suppression by the finite seismogenic layer. *Journal of Geophysical Research*, *115*(B11), B11302. https://doi.org/10.1029/2009jb007122

van den Ende, M. P., & Ampuero, J.-P. (2020). On the statistical significance of foreshock sequences in Southern California. *Geophysical Research Letters*, *47*(3), e2019GL086224. https://doi.org/10.1029/2019gl086224

Wang, K., Dreger, D. S., Tinti, E., Bürgmann, R., & Taira, T. (2020). Rupture process of the 2019 Ridgecrest, California m w 6.4 foreshock and m w 7.1 earthquake constrained by seismic and geodetic data. *Bulletin of the Seismological Society of America*, *110*(4), 1603–1626. https://doi.org/10.1785/0120200108

Wyss, M., & Brune, J. N. (1967). The Alaska earthquake of 28 march 1964: A complex multiple rupture. *Bulletin of the Seismological Society of America*, *57*(5), 1017–1023. https://doi.org/10.1785/bssa0570051017

Xu, S., Fukuyama, E., & Yamashita, F. (2019). Robust estimation of rupture properties at propagating front of laboratory earthquakes. *Journal of Geophysical Research: Solid Earth*, *124*(1), 766–787. https://doi.org/10.1029/2018JB016797

Yamashita, T. (2000). Generation of microcracks by dynamic shear rupture and its effects on rupture growth and elastic wave radiation. *Geophysical Journal International*, *143*(2), 395–406. https://doi.org/10.1046/j.1365-246x.2000.01238.x

Yao, D., Huang, Y., Peng, Z., & Castro, R. R. (2020). Detailed investigation of the foreshock sequence of the 2010 Mw 7.2 El Mayor-Cucapah earthquake. *Journal of Geophysical Research: Solid Earth*, *125*(6), e2019JB019076. https://doi.org/10.1029/2019jb019076

Yoon, C. E., Yoshimitsu, N., Ellsworth, W. L., & Beroza, G. C. (2019). Foreshocks and mainshock nucleation of the 1999 Mw 7.1 Hector Mine, California, earthquake. *Journal of Geophysical Research: Solid Earth*, *124*(2), 1569–1582. https://doi.org/10.1029/2018jb016383

Yue, H., Sun, J., Wang, M., Shen, Z., Li, M., Xue, L., et al. (2021). The 2019 Ridgecrest, California earthquake sequence: Evolution of seismic and aseismic slip on an orthogonal fault system. *Earth and Planetary Science Letters*, *570*, 117066. https://doi.org/10.1016/j.epsl.2021.117066

References From the Supporting Information

Aki, K. (1965). Maximum likelihood estimate of b in the formula log n = a-bm and its confidence limits. *Bulletin of the Earthquake Research Institute, University of Tokyo*, *43*, 237–239.

Aki, K., & Richards, P. G. (2002). *Quantitative seismology*.

Backus, G., & Mulcahy, M. (1976a). Moment tensors and other phenomenological descriptions of seismic sources–I. continuous displacements. *Geophysical Journal International*, *46*(2), 341–361. https://doi.org/10.1111/j.1365-246x.1976.tb04162.x

Backus, G., & Mulcahy, M. (1976b). Moment tensors and other phenomenological descriptions of seismic sources–II. discontinuous displacements. *Geophysical Journal International*, *47*(2), 301–329. https://doi.org/10.1111/j.1365-246x.1976.tb01275.x

Ellsworth, W. L. (2019). From foreshocks to mainshocks: Mechanisms and implications for earthquake nucleation and rupture propagation. *Mechanics of Earthquake Faulting*, *202*, 95.

Magistrale, H. (2002). Relative contributions of crustal temperature and composition to controlling the depth of earthquakes in southern California. *Geophysical Research Letters*, *29*(10), 87-1–87-4. https://doi.org/10.1029/2001gl014375

Rolandone, F., Bürgmann, R., & Nadeau, R. (2004). The evolution of the seismic-aseismic transition during the earthquake cycle: Constraints from the time-dependent depth distribution of aftershocks. *Geophysical Research Letters*, *31*(23), L23610. https://doi.org/10.1029/2004gl021379

Shcherbakov, R., Turcotte, D. L., & Rundle, J. B. (2004). A generalized Omari's law for earthquake aftershock decay. *Geophysical Research Letters*, *31*(11), L11613. https://doi.org/10.1029/2004gl019808